Available online at www.sciencedirect.com
ScienceDirect
Sensors and Actuators B 132 (2008) 418–425
SENSORS AND ACTUATORS B CHEMICAL
www.elsevier.com/locate/snb

Label-free imaging of cancer cells using photonic crystal biosensors and application to cytotoxicity screening of a natural compound library

Leo L. Chan [a,*], Saujanya L. Gosangari [b,c], Kenneth L. Watkin [b,c], Brian T. Cunningham [a]

[a] *Department of Electrical and Computer Engineering, University of Illinois at Urbana-Champaign, United States*
[b] *Beckman Institute for Advanced Science and Technology, Bio-imaging Science and Technology Group, University of Illinois at Urbana-Champaign, United States*
[c] *Department of Speech and Hearing Science, University of Illinois at Urbana-Champaign, United States*

Available online 26 October 2007

Abstract

A rapid and accurate quantitative method for screening the effects of drug compounds upon cells utilizing label-free photonic crystal optical biosensors incorporated within 96-well microplates is described. The biosensors and associated imaging detection instrument enable visualization and quantitative measurement of cell populations attached to the sensor surface with sensitivity sufficient for the detection of individual cells without the use of labels or stains that typically induce the death of the cells under study. The detection method allows repeated measurement of the same cells without removing them from their culture environment, and thus allows direct determination of proliferation and apoptosis rates. In this work, a biosensor-based cell assay is used to screen the effect of a 61-member compound library of plant extracts upon human breast cancer cells, in which some members of the library are shown to induce apoptosis, while others increase the rate of cancer cell proliferation. The results are broadly applicable to a wide range of cell types and compounds, while the assay is simpler and more rapid than alternative apoptosis/proliferation assays.

Keywords: Label-free; Photonic crystal; Microplate; MCF-7; Cytotoxicity; Apoptosis; Imaging

1. Introduction

In the field of pharmaceutical research, the ability to rapidly assess the effects of potential drug compounds upon cells is an important capability for determining which compounds may hold promise for selective cytotoxicity for undesirable cell populations while remaining nontoxic to healthy cells. The most desirable traits of such methods include ease-of-usage, low cost per assay, and the ability to quantitatively screen large populations of cells. The most commonly used methods for detecting cells involve the use of stains or fluorescent labels that allow them to be easily visualized in an optical microscope, fluorescent microscope, or flow cytometry [1]. The shortcoming of the colored staining methods is that the observed cells either do not retain their function or are killed by the staining process, while fluorophores only allow a brief period of observation over a small surface area before the onset of quenching. While flow cytometry enables more quantitative study of fluorophore-labeled cells than microscope-based methods, the cells must be removed from their growth environment for measurement, and the ability to study cell–drug interactions with high throughput is limited. Therefore, the ability to detect cells without the use of fluorescent labels or stains would allow direct repeated observation of cells within their growth media, and enable study of processes such as proliferation, chemotaxis, and death.

Because cells exhibit increased dielectric permittivity with respect to their liquid media [2], they may be easily detected without labels by several types of optical biosensors when the cells become attached to the transducer surface. However, the most common optical biosensors, based upon surface plasmon resonance (SPR) in the Kreitchman configuration [3,4], lack the ability to generate images of cells attached to the sensor surface, while imaging SPR [5–7] methods generate images of only a small area. These limitations, along with those imposed by microfluidic channel-based methods for interfacing the test sample to sensor, such as flow channel blockage and lack of incu-

* Corresponding author at: Department of Electrical and Computer Engineering, University of Illinois at Urbana-Champaign, 208 North Wright Street #257, Urbana, IL 61801, United States. Tel.: +1 2177663035.
E-mail address: lchan1@uiuc.edu (L.L. Chan).

0925-4005/$ – see front matter © 2007 Elsevier B.V. All rights reserved.
doi:10.1016/j.snb.2007.10.027

bation, have resulted in few applications of optical biosensors in the field of cell-based assays.

In contrast to SPR, we have demonstrated cell detection with a photonic crystal optical biosensor that is incorporated into standard 96-well microplates [8] and an imaging detection instrument that enables spatial maps of the attached cell density in the bottom of the microplate wells to be measured by detecting the local changes in the reflection spectrum provided by the photonic crystal. The capability for image-based label-free detection of cell attachment to the sensor was used to visualize the attachment of Jurkat cells to ahCD3 [8].

In this work, the photonic crystal biosensor method is used to screen the effects of a small library of chemical compounds derived from plant extracts with unknown function upon the MCF-7 human breast cancer cell line. Using the 96-well assay format and the imaging detection instrument, the biosensor assay provides images of the density distribution of cells attached to the wells and quantitative determination of cell count and rate of proliferation/death. The assay is used to rapidly differentiate plant extracts that either enhance the rate of cell proliferation relative to a negative control or that result in cytotoxicity relative to a positive control.

2. Materials and methods

2.1. Sensor and instrument

The photonic crystal biosensors used in this work have been described in previous publications [9,10], but their design and operation will be briefly summarized. The sensor is comprised of a one-dimensional periodic grating surface structure (period = 550 nm) formed within a UV-cured polymer on a transparent polyester sheet using a room-temperature replica molding process. The low refractive index grating is subsequently coated with a film of high refractive index TiO_2 by sputtering to achieve the finished device structure. The biosensors are cut from the polyester sheet and attached with adhesive to form the bottom surface of standard 96-well format microplates [11]. The device behaves as a narrowband wavelength reflectance filter, where the sensor reflects ~100% of incident light at the resonant wavelength, while all other wavelengths are transmitted through the sensor structure.

The sensor operates by measuring local changes in the wavelength of reflected light as cellular binding events take place within an evanescent field region adjacent to the surface. The resonant reflected wavelength of the sensor can be measured by illuminating the photonic crystal at normal incidence with white light, and collecting the reflected light with a spectrometer. Image-based detection with high spatial resolution is enabled by the photonic crystal structure, which is designed to cut off lateral propagation of the resonant wavelength, thus eliminating pixel-to-pixel optical cross-talk.

The detection instrument (SRU Biosystems), previously described [9,11], illuminates the sensor surface at normal incidence with a white light lamp, and a line from the sensor surface is imaged into the entrance slit of an imaging spectrometer. The reflected spectrum of each pixel across the image line is gathered, and the peak wavelength value (PWV) of each resonant reflection spectrum is mathematically determined. A PWV image is constructed by sequential scanning of the sensor across the imaged line region in 22.3 μm increments. The detection instrument measures changes in the resonant reflected PWV of the biosensor surface as the detected output on a pixel-by-pixel basis that can generate images of PWV with a spatial resolution as low as 4 μm × 4 μm. An imaging resolution of 22.3 μm × 22.3 μm was used for all the images reported in this work, as higher resolution scans require time and computer memory in proportion to number of image pixels. Detection of cell attachment to the sensor requires measuring a shift in PWV, so the sensor surface must be scanned two times: once before and once after cells have been immobilized on the surface. The two images are automatically aligned (using incorporated alignment features) and mathematically subtracted by software to determine the difference in PWV on the sensor surface between the two scans. Because the PWV is only increased for pixels in which a cell has attached to the sensor, the imaging instrument measures the density of cell binding as a function of position within the microplate well. The method has been shown to be capable of detecting the attachment of individual cells, and for scanning large populations of cells attached within all the wells of the microplate [8,12].

2.2. MCF-7 cell line and plant extracts preparation

The human breast cancer cell line MCF-7 cells were cultured in minimum essential medium with 10% fetal bovine serum and antibiotic–antimycotic (American Type Culture Collection (ATCC)). The cells were maintained in an incubator at 37 °C with 5% carbon dioxide.

The 61 different plant extracts (Table 1) were provided by Professor R. Chowdhury from University of Dhaka, Bangladesh. Some of the same plant species are extracted by various methods shown in Table 1. Stock solutions of the plant extracts were prepared by dissolving them in ethanol at 25 mg/ml. The plant extracts were diluted with cell culture media to a concentration of 100 μg/ml, so that the final concentration of ethanol was less than 1% in sample solution.

2.3. MCF-7 cancer cell detection protocol and cell counting method

The assay protocol is outlined in Fig. 1. A baseline PWV image is initially scanned (Scan "A") with the biosensor microplate wells filled with 100 μl cell culture media. Approximately 500–1000 cells are then introduced to each well and allowed to immobilize to the sensor surface for ~24 h in a CO_2 incubator. A second PWV image is scanned (Scan "B") after the cells have attached to the sensor surface. Subtraction of Scan "A" from Scan "B" generates a PWV shift image that measures the distribution of attached cells. Next, the plant extract solutions are exposed to the cells, and the microplate is returned to the incubator for an additional 24 h before a third PWV image is scanned (Scan "C"). Subtraction of Scan "A" from Scan "C" generates a new PWV shift image of the cell distribution. Cell proliferation and death can be observed by comparing Scan (B–A) and Scan

Table 1
The 61 different plant species and the method of extraction

No.	Name	Extract/partitionate
1	*Aglaia roxburghiana*	*n*-Hexane partitionate of MeOH extract
2	*Alternanthera sessilis*	Pet-ether fraction of MeOH extract
3	*Alternanthera sessilis*	MeOH residue of MeOH extract
4	*Alternanthera sessilis*	$CHCl_3$ fraction of MeOH extract
5	*Amoora chittagonga*	Pet-ether partitionate of MeOH extract
6	*Amoora chittagonga*	$CHCl_3$ partitionate of MeOH extract
7	*Amoora chittagonga*	EtOAc partitionate of MeOH extract
8	*Amoora cucullata*	MeOH extract
9	*Amoora rohituka*	Pet-ether extract
10	*Amoora rohituka*	MeOH extract
11	*Anisoptera glabra*	MeOH extract
12	*Anogeissus latifolia*	EtOH extract
13	*Brunfelsia americana*	MeOH extract
14	*Brunfelsia latifolia*	MeOH extract
15	*Buchanania lanzen*	MeOH extract
16	*Bursera serrata*	Pet-ether extract
17	*Bursera serrata*	Dichloromethane extract
18	*Chukrasia tabularis*	MeOH extract
19	*Cinnamomum zeylanicum*	MeOH extract
20	*Citrus hystrix*	MeOH extract
21	*Combretum coccineum*	$CHCl_3$ partitionate of acidified MeOH extract
22	*Combretum gradiflorum*	MeOH extract
23	*Eclipta prostata*	MeOH extract
24	*Eiroglossum edule*	MeOH extract
25	*Ficus* sp.	MeOH extract
26	*Garuga pinnata*	MeOH extract
27	*Indigofera tinctoria*	EtOH extract
28	*Lannea coromandelica*	MeOH extract
29	*Nephelium litchi*	MeOH extract
30	*Nephelium longum*	MeOH extract
31	*Pesprum nocturnum*	MeOH extract
32	*Petunia meleagris*	MeOH extract
33	*Petunia phoenica*	MeOH extract
34	*Petunia punctata*	MeOH extract
35	*Petunia violaceae*	MeOH extract
36	*Phyllanthus reticulatus*	$CHCl_3$ fraction of MeOH extract
37	*Phyllanthus reticulatus*	$CHCl_3$ fraction of pet-ether extract
38	*Phyllanthus reticulatus*	Hexane fraction of CH_2Cl_2 extract
39	*Phyllanthus reticulatus*	Acidified $CHCl_3$ fraction of aqueous extract
40	*Phyllanthus reticulatus*	Acetone extract
41	*Poivrea coccinea*	MeOH extract
42	*Pongamia glabra*	MeOH extract
43	*Protium serratum*	MeOH extract
44	*Pterospermum suberifolium*	MeOH extract
45	*Quisqualis indica*	Pet-ether extract
46	*Quisqualis indica*	MeOH extract
47	*Sapindus mukurossi*	MeOH extract
48	*Semecarpus anacardium*	MeOH extract
49	*Shorea robusta*	EtOH extract
50	*Solanum ferox*	MeOH extract
51	*Solanum indicum*	MeOH extract
52	*Spondias mangifera*	MeOH extract
53	*Swintonia floribunda*	MeOH extract
54	*Terminalia bellerica*	MeOH extract
55	*Terminalia bellerica*	MeOH extract
56	*Trachyspermum ammi*	EtOH extract
57	*Xanthoxylum budrunga*	MeOH residue of MeOH extract
58	*Xanthoxylum budrunga*	Pet-ether fraction of MeOH extract
59	*Xylocurpus mollucensis*	*n*-Hexane partitionate of MeOH extract
60	*Xylocurpus mollucensis*	MeOH residue of MeOH extract
61	*Zizyphus jujuba*	MeOH extract

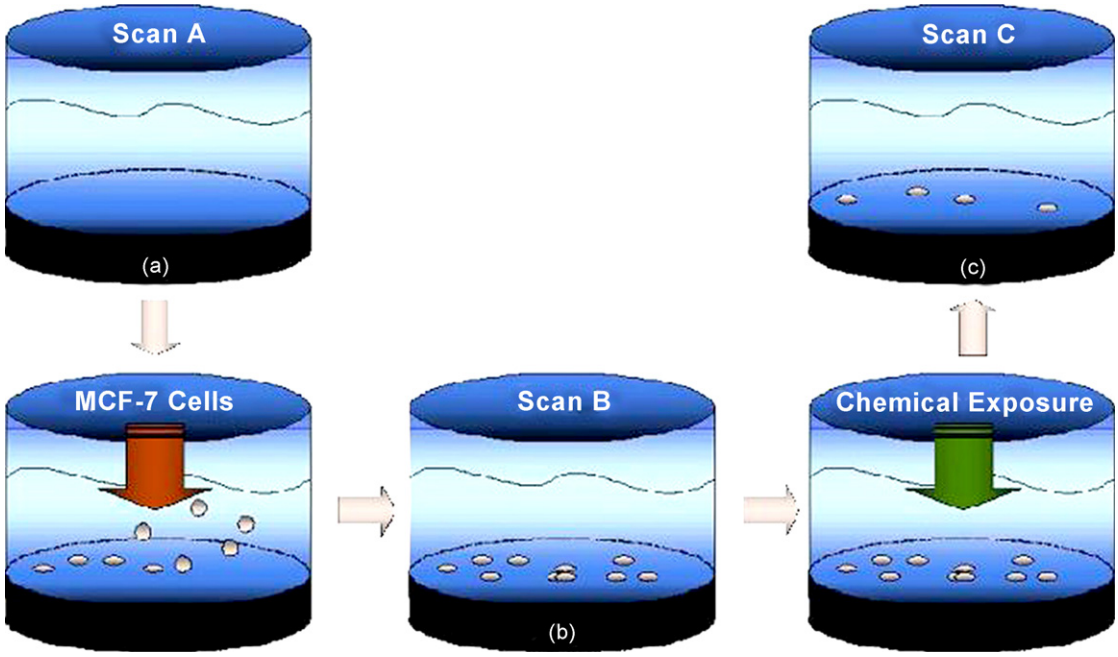

Fig. 1. Cell cytotoxicity assay protocol: (a) a baseline is scanned with cell culture media in the wells, and the MCF-7 cells are allowed to incubate in the wells for 24 h, (b) a cell immobilization image is scanned, and the cells are exposed to 61 plant extracts for another 24 h, and (c) a final image is scanned with the remaining cells in the wells.

(C–A). All conditions were measured with triplicate wells, and wells without chemical compound introduction were utilized as experimental controls.

In order to estimate the number of cells attached to the sensor surface, we apply a PWV shift threshold to the pixels collected in the PWV shift image to separate and disregard lower PWV pixels while counting only the locally higher PWV pixels. For each well, a histogram is used to visualize the proportion of pixels with a PWV shift above the selected threshold. For this work, the pixels above the threshold are counted as a single cell, thus it is possible that this simple algorithm would undercount cells for pixels with large PWV shift due to multiple cells/pixel. A cell count value was determined for each well before and after incubation of the cells with the plant extract compounds, and the percentage change of cell count during the incubation period was calculated.

3. Results

The plant extracts were screened simultaneously with triplicate negative controls (no drug compound present) and positive controls (*doxorubicin* and *curcumin*). The negative controls were measured by allowing the MCF-7 cells to incubate and grow without drug compound for 24 h, which resulted in an average proliferation rate of 92.29% ± 30.61/day (Thus, a 100% proliferation rate represents a doubling of the cell count). The positive controls were measured by allowing the MCF-7 cells to incubate in 100 μM of *doxorubicin* and *curcumin* solutions for 24 h, which resulted in an average death rate of −89.65% ± 7.41 and −92.92% ± 4.48/day, respectively (Thus, a −100% death rate represents complete loss of all the original cells).

The screening of 61 plant extracts revealed several distinct types of behavior within the MCF-7 cancer cells. The effects may be divided into five categories: (1) no effect (rate of proliferation is within ±20% of the negative control), (2) enhanced proliferation (rate of proliferation ≥20% higher than the negative control), (3) reduced proliferation (rate of proliferation ≥20% lower than the negative control, but still proliferating), (4) cytotoxic (cell death rate ≥10% lower than the positive control), and (5) highly cytotoxic (cell death rate within 10% of the positive control). Biosensor images of representative individual wells from each category before and after the compound incubation period are shown in Fig. 2.

Fig. 2a shows the PWV images after the initial cell incubation (left image) and after the same cells are allowed to proliferate for 24 h (right image) without the presence of a compound. The images show distinct regions with pixels displaying an elevated PWV with respect to the PWV of the background due to the attachment of cells to the biosensor. Because each pixel of the image represents a ~22.3 μm × 22.3 μm region of the biosensor surface, attachment of an individual cell within a region corresponding to one pixel results in an elevated PWV measured for only one pixel, and many single-pixel cells are observed. The cells also have a tendency to group within clusters, and clusters are distributed in random patterns within the well. Within a cluster, a single pixel may hold more than one cell, and pixels within clusters are observed to register a higher PWV shift than individual cells. Regions with locally elevated PWV for both cell clusters and individual cells are observed to grow in size with time. It is important to note that regions with elevated PWV represent cells that have formed a close physical attachment to the biosensor surface, and that dead cells—even if physically deposited on the same sensor surface—do not reg-

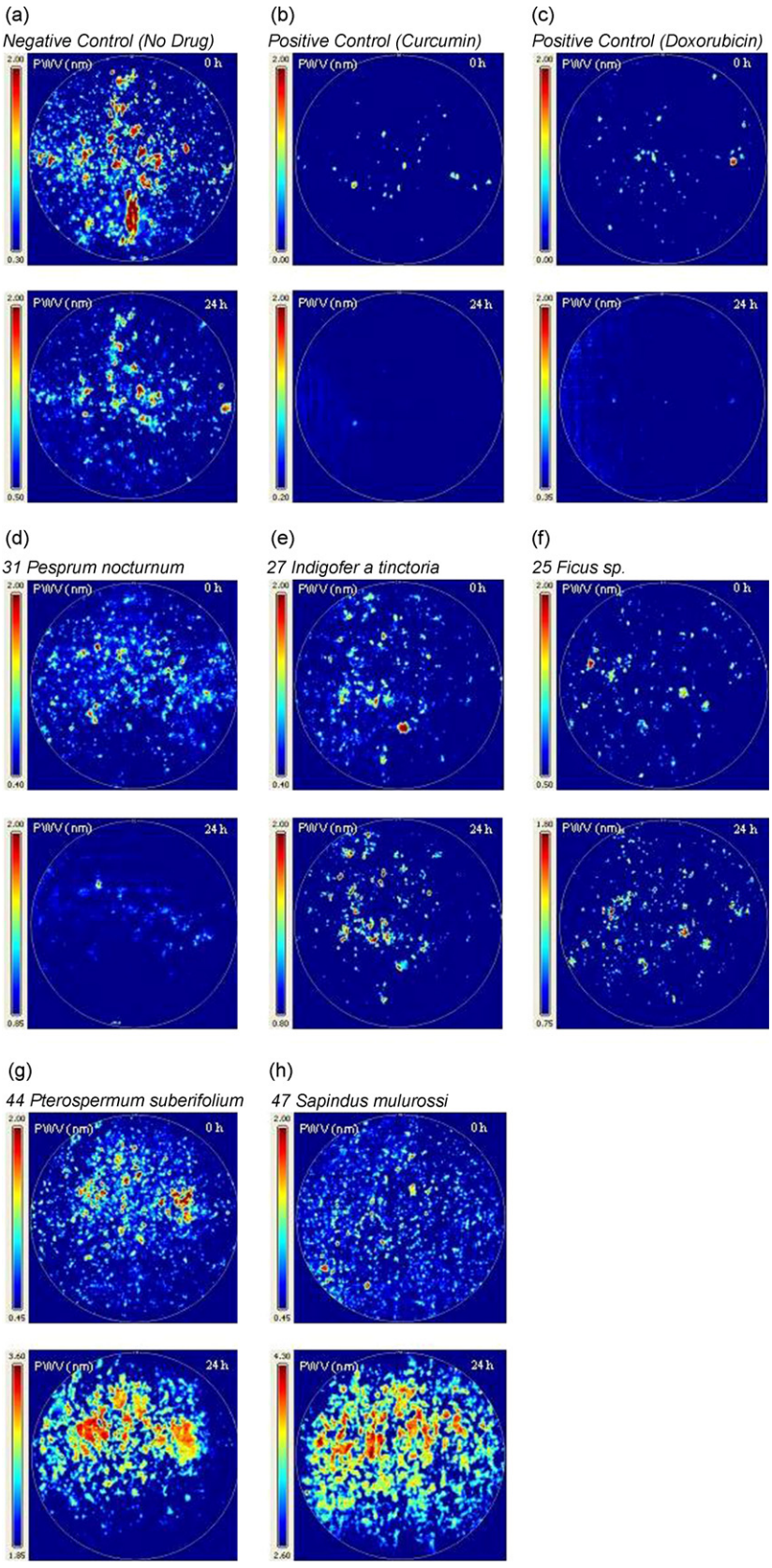

Fig. 2. Examples of PWV shift images are shown, with PWV shift scale bars indicating the magnitude of the wavelength shift in units of nanometers. Pixels with greater PWV shift are displayed with brighter colors, and indicate locations in which cancer cell attachment occurs. The five categories of the results are shown, (a) the negative control (no drug compound present), (b) the positive control (*curcumin*), (c) the positive control (*doxorubicin*), (d) "highly cytotoxic" (*Pesprum nocturnum*), (e) "cytotoxic" (*Indigofera tinctoria*), (f) "reduced proliferation" (*Ficus* sp.), (g) "no effect" (*Pterospermum suberifolium*), and (h) "enhanced proliferation" (*Sapindus mukurossi*) both before and (left image) after (right image) a 24 h incubation period.

Table 2
List of plant extracts divided into five categories, "highly cytotoxic", "cytotoxic", "reduced proliferation", "no effect", and "enhanced proliferation". The table is ranked from the most cytotoxic to the most proliferative plant extract. The last column represents the percentage of cell cytotoxicity and proliferation for each plant extract, where negative values correspond to cytotoxicity, and positive percentage represents proliferation

Name	No.	Effects	Average% cell cytotoxicity/proliferation
Trachyspermum ammi	56	Highly cytotoxic	−0.97
Xylocurpus mollucensis	60	Highly cytotoxic	−0.97
Eiroglossum edule	24	Highly cytotoxic	−0.96
Pesprum nocturnum	31	Highly cytotoxic	−0.95
Phyllanthus reticulatus	36	Highly cytotoxic	−0.95
Petunia phoenica	33	Highly cytotoxic	−0.93
Xanthoxylum budrunga	58	Highly cytotoxic	−0.93
Curcumin		**Positive control**	−0.93
Amoora chittagonga	6	Highly cytotoxic	−0.92
Anogeissus latifolia	12	Highly cytotoxic	−0.92
Chukrasia tabularis	18	Highly cytotoxic	−0.92
Phyllanthus reticulatus	37	Highly cytotoxic	−0.92
Amoora cucullata	8	Highly cytotoxic	−0.90
Doxorubicin		**Positive control**	−0.90
Aglaia roxburghiana	1	Highly cytotoxic	−0.89
Alternanthera sessilis	4	Highly cytotoxic	−0.85
Amoora rohituka	9	Highly cytotoxic	−0.84
Amoora chittagonga	5	Highly cytotoxic	−0.83
Garuga pinnata	26	Highly cytotoxic	−0.82
Buchanania lanzen	15	Highly cytotoxic	−0.81
Combretum coccineum	21	Cytotoxic	−0.77
Phyllanthus reticulatus	38	Cytotoxic	−0.63
Petunia violaceae	35	Cytotoxic	−0.62
Solanum ferox	50	Cytotoxic	−0.57
Eclipta prostata	23	Cytotoxic	−0.46
Indigofera tinctoria	27	Cytotoxic	−0.45
Solanum indicum	51	Cytotoxic	−0.41
Bursera serrata	17	Cytotoxic	−0.31
Petunia meleagris	32	Cytotoxic	−0.31
Poivrea coccinea	41	Cytotoxic	−0.28
Ficus sp.	25	Reduced proliferation	0.01
Petunia punctata	34	Reduced proliferation	0.01
Terminalia bellerica	55	Reduced proliferation	0.02
Quisqualis indica	46	Reduced proliferation	0.04
Xylocurpus mollucensis	59	Reduced proliferation	0.07
Nephelium longum	30	Reduced proliferation	0.10
Swintonia floribunda	53	Reduced proliferation	0.25
Zizyphus jujuba	61	Reduced proliferation	0.26
Anisoptera glabra	11	Reduced proliferation	0.26
Alternanthera sessilis	3	Reduced proliferation	0.29
Xanthoxylum budrunga	57	Reduced proliferation	0.31
Alternanthera sessilis	2	Reduced proliferation	0.35
Phyllanthus reticulatus	40	Reduced proliferation	0.41
Brunfelsia latifolia	14	Reduced proliferation	0.45
Citrus hystrix	20	Reduced proliferation	0.48
Cinnamomum zeylanicum	19	Reduced proliferation	0.50
Nephelium litchi	29	Reduced proliferation	0.50
Brunfelsia americana	13	Reduced proliferation	0.54
Quisqualis indica	45	Reduced proliferation	0.73
Spondias mangifera	52	Reduced proliferation	0.74
Amoora rohituka	10	No effect	0.79
Phyllanthus reticulatus	39	No effect	0.79
Pterospermum suberifolium	44	No effect	0.89
Bursera serrata	16	No effect	0.90

Table 2 (*Continued*)

Name	No.	Effects	Average% cell cytotoxicity/proliferation
No drug compound		**Negative control**	0.92
Combretum gradiflorum	22	No effect	0.99
Terminalia bellerica	54	No effect	1.02
Protium serratum	43	No effect	1.03
Lannea coromandelica	28	Enhanced Proliferation	1.34
Semecarpus anacardium	48	Enhanced proliferation	1.38
Shorea robusta	49	Enhanced proliferation	1.38
Pongamia glabra	42	Enhanced proliferation	1.59
Sapindus mukurossi	47	Enhanced proliferation	1.83
Amoora chittagonga	7	Enhanced proliferation	2.32

ister an increase in PWV. Fig. 2 also highlights the advantage of using an image-based detection system to perform cell-based assays, as measurement of only a portion of the well could result in large errors in determination of the actual growth rate. Fig. 2b and c demonstrate the effects of cytotoxic chemical compounds. Although the cells are initially attached to the biosensor, induction of apoptosis causes fragmentation of the cells and eventual loss of adhesion, resulting in a biosensor surface that has fewer (or no) attached cells after a 24-h exposure. Example images from the exposure to the plant extract library show the complete range of response between extracts that are nearly as cytotoxic as the positive controls, to extracts that actually accelerate the rate of proliferation. The results of screening, summarized in Table 2 , show that, of the 61 plant extracts, 18 are "highly cytotoxic", 10 are "cytotoxic", 20 result in "reduced proliferation", 7 have "no effect", and 6 result in "enhanced proliferation" according to our previously described definitions. The average standard deviation of the categories is approximately ±10%.

4. Discussion

The screening capability demonstrated in this work is made possible by the combined ability of the biosensor structure to produce a highly localized shift in reflected wavelength at the site of cell attachment, and the ability of the imaging detection instrument to scan a large sensor surface area with sufficient resolution to monitor the attachment/detachment of individual cells. As the biosensor is incorporated into a 96-well format (as opposed to a microfluidic channel) the cells are maintained within their culture environment, where they remain viable for repeated measurements that may extend over the course of several days. The cell attachment images are useful for direct visualization of cell behavior and also readily translated to a simple cell count. Although the method does not have sufficient optical resolution to gather detailed images within a single cell, the method can easily detect a single cell, and is useful for studying large populations of cells.

Using the biosensor assay, we were able to rapidly differentiate and classify the effects of several plant extracts upon cancer cells with previously unknown function. A broad continuum of responses was obtained. While some compounds (including *doxorubicin* and *curcumin*—the positive controls) indeed induced cell death, as detected by cell detachment, others resulted in an increased rate of cell proliferation as compared with the negative control (no drug exposure). The screening procedure presented here represents only one small part of the process of identification of a potential drug treatment. Having identified several compounds with cytotoxic behavior, more detailed dose/response characterization of these compounds must be performed to determine and compare their IC_{50} concentrations (concentration at which the compound is toxic to 50% of the cell population). Further screening must be performed in order to determine the toxicity of selected compounds to non-cancerous cells in order to determine the likelihood of toxic side effects. The photonic crystal biosensor assay protocol described in this work is expected to be useful for these types of studies as well, and will be the topic of future publications.

5. Conclusion

In this work, a label-free photonic crystal biosensor incorporated into a standard 96-well microplate format in conjunction with a high resolution imaging detection instrument is used to study the effects of a small library of chemical compounds derived from plant extracts with unknown function upon MCF-7 human breast cancer cells. The assay provides rapid images of the density distribution of cells attached to the sensor surface and quantitative determination of cell count and rate of proliferation/death. The assay was used to differentiate plant extracts that either enhance the rate of cell proliferation relative to a negative control or that result in cytotoxicity relative to a positive control. Because the method does not use labels or stains, the same population of cells can be measured multiple times without removing them from their culture environment. The system has resolution for detection of individual cells, and yet can gather statistics on large populations of cells. The method is broadly applicable for screening the interaction of many cell types with exposure to potential drug compounds to determine their effect upon proliferation and/or cytotoxicity.

Acknowledgments

This material is based upon work supported by the National Science Foundation under Grant No. 0427657, and by SRU Biosystems. Any opinions, findings, and conclusions or recommendations expressed in this material are those of the author(s) and do not necessarily reflect the views of the National Science Foundation. The authors would like to thank Professor R. Chowdhury from University of Dhaka, Bangladesh for providing the plant extracts. The authors gratefully acknowledge SRU Biosystems for providing the photonic crystal biosensor microplates. The authors also extend their gratitude to the support staff of the Micro and Nanotechnology Laboratory at the University of Illinois at Urbana-Champaign.

References

[1] F. Belloc, P. Dumain, M.R. Boisseau, C. Jalloustre, J. Reiffers, P. Bernard, F. Lacombe, A flow cytometric method using Hoechst-33342 and propidium iodide for simultaneous cell-cycle analysis and apoptosis determination in unfixed cells, Cytometry 17 (1994) 59–65.
[2] M. Zourob, S. Mohr, B.J.T. Brown, P.R. Fielden, M.B. McDonnell, N.J. Goddard, Bacteria detection using disposable optical leaky waveguide sensors, Biosens. Bioelectron. 21 (2005) 293–302.
[3] A. Frutos, S.C. Weibel, R.M. Corn, Near infrared surface plasmon resonance measurements of ultrathin films. 2. Fourier transform SPR spectroscopy, Anal. Chem. 71 (1999) 3935–3940.
[4] J.S. Yuk, S.-J. Yi, H.G. Lee, H.J. Lee, Y.-M. Kim, K.-S. Ha, Characterization of surface plasmon resonance wavelength by changes of protein concentration on protein chips, Sens. Actuators B 94 (2003) 161–164.
[5] C.E. Jordan, R.M. Corn, Surface plasmon resonance-imaging measurements of electrostatic biopolymer adsorption onto chemically modified gold surfaces, Anal. Chem. 69 (1997) 1449–1456.
[6] B.P. Nelson, T.E. Grimsrud, M.R. Liles, R.M. Goodman, R.M. Corn, SPR imaging measurements of DNA and RNA hybridization adsorption onto DNA microarrays, Anal. Chem. 73 (2001) 1–7.
[7] E.A. Smith, R.M. Corn, SPR imaging as a tool to monitor biomolecular interactions in an array-based format, Appl. Spectrosc. 57 (2003) 320A–322A.
[8] B. Lin, P. Li, B.T. Cunningham, A label-free biosensor-based cell attachment assay for characterization of cell surface molecules, Sens. Actuators B: Chem. 114 (2006) 559–564.
[9] B.T. Cunningham, P. Li, B. Lin, J. Pepper, Colorimetric resonant reflection as a direct biochemical assay technique, Sens. Actuators B 81 (2002) 316–328.
[10] A.J. Haes, R.P.V. Duyne, A nanoscale optical biosensor: sensitivity and selectivity of an approach based on the localized surface plasmon resonance spectroscopy of triangular silver nanoparticles, J. Am. Chem. Soc. 124 (2002) 10596–10604.
[11] B.T. Cunningham, P. Li, S. Schulz, B. Lin, C. Baird, J. Gerstenmaier, C. Genick, F. Wang, E. Fine, L. Laing, Label-free assays on the BIND system, J. Biomol. Screen 9 (2004) 481–490.
[12] B.T. Cunningham, L. Laing, Microplate-based, label-free detection of biomolecular interactions: applications in proteomics, Expert Rev. Proteomics 3 (2006) 271–281.

Biographies

Leo Li-Ying Chan is a graduate research assistant at the University of Illinois at Urbana-Champaign in the Nano-Sensors Group directed by Dr. Brian T. Cunningham. His research focuses on the characterization of photonic crystal optical biosensors and the optimization of small molecule biodetection using this platform. Before joining Dr. Cunningham's group, Leo Chan served as an undergraduate research at Keck Graduate Institute, Claremont, California, where he worked on the application of free solution electrophoresis to DNA finger printing. He earned his BS and MS in electrical and computer engineering with a minor in biomedical engineering from the University of Illinois at Urbana-Champaign, where he is currently pursuing a PhD.

Saujanya Gosangari is a graduate research assistant at the University of Illinois at Urbana-Champaign with the Bioimaging Science and Technology Group at the Beckman Institute. She is currently pursuing a PhD in speech and hearing sciences and her research focuses on the development of targeted drug delivery systems for the treatment of oro-pharyngeal cancers. Saujanya has a Masters degree in electrical engineering from State University of New York, Stony Brook. She earned her undergraduate degree in electronics engineering from University of Mumbai, India.

Kenneth Lloyd Watkin is a professor of speech and hearing science and a professor of medicine at the University of Illinois, where he is the director of the Medical Imaging Research Laboratory. He is also director of the Targeting Imaging Laboratory in the Bioimaging Sciences and Technology Group at the Beckman Institute for Advanced Science and Technology as well as a research fellow at the National Center for Supercomputing Applications. His research groups focus on neuro-imaging of the brain, development of multimodal contrast agents for the imaging and treatment of cancer, as well as the development of biosensors and systems for medical monitoring. Dr. Watkin earned his BS from the University of Puget Sound and his MS, and PhD degrees from the University of Washington. His postdoctoral work was conducted in medical physics and engineering at the University of Wisconsin, Madison. His thesis research was in the field of medical image analysis, where his contributions include to the development of 3D imaging hardware and software that is now widely used in diagnostic medicine.

Brian T. Cunningham is an associate professor of electrical and computer engineering at the University of Illinois at Urbana-Champaign, where he is the director of the Nano-Sensors Group. His group focuses on the development of photonic crystal-based transducers, plastic-based fabrication methods, and novel instrumentation approaches for label-free biodetection. Prof. Cunningham is a founder and the Chief Technical Officer of SRU Biosystems (Woburn, MA), a life science tools company that provides high sensitivity plastic-based optical biosensors, instrumentation, and software to the pharmaceutical, academic research, genomics, and proteomics communities. Prior to founding SRU Biosystems in June 2000, Dr. Cunningham was the Manager of Biomedical Technology at Draper Laboratory (Cambridge, MA), where he directed R&D projects aimed at utilizing defense-related technical capabilities for medical applications. In addition, Dr. Cunningham served as Group Leader for MEMS Sensors at Draper Laboratory, where he directed a group performing applied research on microfabricated inertial sensors, acoustic sensors, optical switches, microfluidics, tissue engineering, and biosensors. Concurrently, he was an associate director of the Center for Innovative Minimally Invasive Therapy (CIMIT), a Boston-area medical technology consortium, where he led the Advanced Technology Team on Microsensors. Before working at Draper Laboratory, Dr. Cunningham spent 5 years at the Raytheon Electronic Systems Division developing advanced infrared imaging array technology for defense and commercial applications. Dr. Cunningham earned his BS, MS, and PhD degrees in electrical and computer engineering at the University of Illinois. His thesis research was in the field of optoelectronics and compound semiconductor material science, where he contributed to the development of crystal growth techniques that are now widely used for manufacturing solid-state lasers, and high frequency amplifiers for wireless communication.